Japanese Journal of Applied Physics
Vol. 45, No. 5B, 2006, pp. 4718–4721

Spatial Distribution Measurement of Heart Wall Vibrations Generated by Remote Perturbation of Inner Pressure

Hiroshi KANAI*, Hideyuki HASEGAWA and Kohsuke IMAMURA

Department of Electronic Engineering, Graduate School of Engineering, Tohoku University, Aramaki-aza-Aoba 6-6-05, Sendai 980-8579, Japan

(Received November 30, 2005; accepted February 13, 2006; published online May 25, 2006)

It is essential for the diagnosis of heart diseases to noninvasively measure instantaneous myocardial movability and transition properties during one cardiac cycle. This study proposes a novel method of noninvasively perturbing left ventricle (LV) internal pressure by *remotely actuating* the brachium artery with sinusoidal vibration for the diagnosis of myocardial movability. By attaching an actuator to the brachium artery and driving it with a sinusoidal wave of f_0 Hz, the internal pressure of the artery is perturbed. The perturbation propagates along the artery to the LV of the heart and the sinusoidal perturbation of the LV internal pressure is induced. Using an ultrasound-based phased tracking method, the resultant minute motion of the heart wall can be noninvasively measured. Because the *vibration mode* of the heart wall depends on actuation frequency, by phantom experiments using a spherical shell made of silicone rubber, to which a silicone rubber tube is connected, the vibration mode was identified from the measurement of the spatial distribution of the motions by scanning with an ultrasonic beam. From an *in vivo* experiment, the principle of remote actuation was confirmed. [DOI: 10.1143/JJAP.45.4718]

KEYWORDS: phased tracking method, myocardium vibration, myocardium movability, remote actuation, viscoelasticity, tissue characterization, internal pressure, vibration mode

1. Introduction

Though myocardial movability is important in the diagnosis of heart diseases,[1–3] a non-invasive method of estimating *the movability* has never been developed. The viscoelasticity of the heart wall is estimated by the ratio of the applied change in internal pressure to the resultant strain in the heart wall. However, because large vibration components are contaminated by the heart wall vibration naturally generated by a heartbeat, ultrasound-based actuation[4–6] cannot easily be applied under safety guidelines.

When the heart wall is sinusoidally actuated using a large-scale *low-frequency* actuator directly attached to the chest wall, the bending vibration (mode 2) dominantly occurs in the heart wall as shown in Fig. 1(c). For mode-2 vibration, however, there are eight nodes that do not move on the heart wall. Thus, it is necessary to distinguish these nodes from the diseased regions to avoid underestimating the movability of the myocardial region. For this purpose, it is necessary to select an actuation frequency f_0 so that vibration with mode 0 [as in Fig. 1(a)], where the node is not included, is actuated.

In our laboratory, the change in the internal pressure of the common carotid artery (CCA) was generated by remote cyclic actuation at the brachium artery and the elastic modulus of the CCA wall was measured by an ultrasound-based method at multiple frequencies in basic[7] and *in vivo* experiments[8] to non-invasively estimate the viscoelasticity of the arterial wall.[9]

In this study, *remote actuation* is applied so that the internal pressure of the left ventricle (LV) is successfully perturbed in *in vivo* experiments. At the same time, the velocity signals on the interventricular septum (IVS) are measured using the ultrasound-based *phased tracking method*.[10,11] Prior to the *in vivo* experiments, using a phantom of a silicone rubber shell similar in size and elasticity to an actual heart of a typical healthy adult, f_0 is predetermined in phantom experiments so that vibration with mode 0 is generated. There is not node in mode-0 vibration. This method has a potential for non-invasively evaluating myocardial movability and the transition properties of the heart wall during one cardiac cycle.

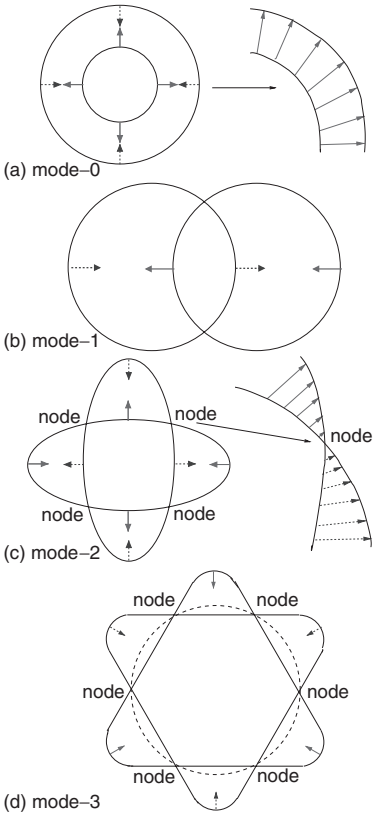

Fig. 1. Each vibration mode with spherical shell.

2. Principle of *In Vivo* Actuation

As shown in Fig. 2, by attaching a large-scale low-frequency actuator to the right brachium artery and driving it with a sinusoidal wave of f_0 Hz (approximately 10 Hz), the internal pressure of the artery is perturbed and the perturbation propagates along the artery to the LV of the

*E-mail address: kanai@ecei.tohoku.ac.jp

Fig. 2. Photograph of *in vivo* experiments in which right brachium artery is actuated with large scale actuator and velocity waves on heart wall are measured.

heart through the aortic valve. Then, the sinusoidal perturbation of the LV internal pressure is generated. Using an ultrasound-based phased tracking method,[10,11] the resultant minute motion of the heart wall can be measured. Because the *vibration mode* of the heart wall depends on f_0, myocardial movability cannot be correctly measured at nodes. Thus, the generation of the vibration with mode 0, which does not include nodes, is essential. For the actual heart, however, because there are large motion components due to a heartbeat, it is not easy to accurately detect the spatial distribution of the minute wall motion caused by remote actuation at present. In particular, for the LV posterior wall, because data at points deep in the skin is required, frame rate cannot be increased and accurate measurement is not easily realized. For the above purpose, therefore, by the basic experiments described in the next section, the f_0 of vibration with mode 0 is predetermined in phantom experiments from the measurement of the spatial distribution of heart wall motion by scanning with an ultrasonic beam.[12,13]

3. Basic Experiments Using Silicone Shell

As a model of the heart of a typical healthy adult, we used a spherical shell (outer diameter = 45 mm, thickness = 7.5 mm) made of silicone rubber (Toshiba YE5623) and set in a water tank as shown in Fig. 3. A silicone rubber tube (50 cm long) was connected to the spherical shell. The shell and tube were filled with water. By remotely actuating the tube using a large-scale actuator with a sinusoidal vibration of f_0 Hz, the internal pressure of the shell was perturbed at several mmHg. According to the mechanical test, the elasticity of the silicone rubber was approximately 46 kPa at 10 Hz, which is similar to the elasticity of the heart wall of a healthy young subject measured in *in vivo* experiments (approximately 30 kPa for 10–90 Hz).[13] The LV is mainly supported by the aorta. Thus, the boundary condition of the phantom in the experiment is similar to that of the actual heart.

As shown in the lower inset of Fig. 3, for measuring the spatial distribution of the velocity wave on the shell walls, the ultrasonic probe was set at one of three positions (A, B, and C) using the *x*-stage. For each position, the ultrasonic

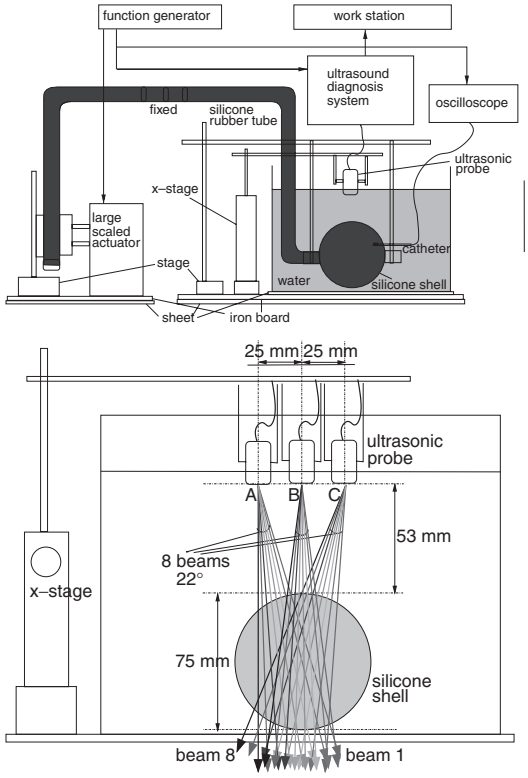

Fig. 3. Upper: Setup for basic experiment, in which internal pressure of silicone spherical shell was perturbed and spatial distribution of velocity waves along shell surface was measured by scanning ultrasonic beams. Lower: For measuring spatial distribution of velocity wave on shell walls, ultrasonic probe was set at one of three positions (A, B, C) using *x*-stage and ultrasonic beam was scanned sparsely in eight directions at each position.

beam was scanned sparsely in eight directions. Thus, remotely actuated vibrations were measured at 24 points on the anterior wall and at 24 points on the posterior wall of the shell. By referring to the actuation signal, the phases in all these measured vibration signals were matched.

Figure 4 shows the waveforms of the velocity signals simultaneously measured at eight points on the anterior wall and at eight points on the posterior wall by setting the probe at position C. In both walls, there were spatial changes in the phase of the actuated pressure perturbation signal along the wall surface.

At 18 ms in Fig. 4, the amplitudes of each waveform at 48 points along the walls were detected. The results are shown for $f_0 = 17$ Hz in the upper inset of Fig. 5 and for $f_0 = 30$ Hz in the lower inset of Fig. 5. From the measured spatial distribution of the vibrations on the shell surface, the vibration mode was identified. That is, for $f_0 = 17$ Hz, the vibration mode is mode 2, whereas for $f_0 = 30$ Hz, the vibration mode is similar to mode 3.

Figure 6 shows the frequency characteristics of the maximum amplitude of the velocity waveform. For $f_0 =$ 7–8 Hz, the vibration-mode is 0, which indicates the homogeneous expansion and contraction of the shell wall without any nodes as shown in Fig. 1(a). For 12 Hz, the vibration mode is 1, which indicates the parallel displacement of the whole shell, as shown in Fig. 1(b). For $f_0 =$ 16–17 Hz, the vibration mode is 2. From this distribution, the positions of the nodes were identified.

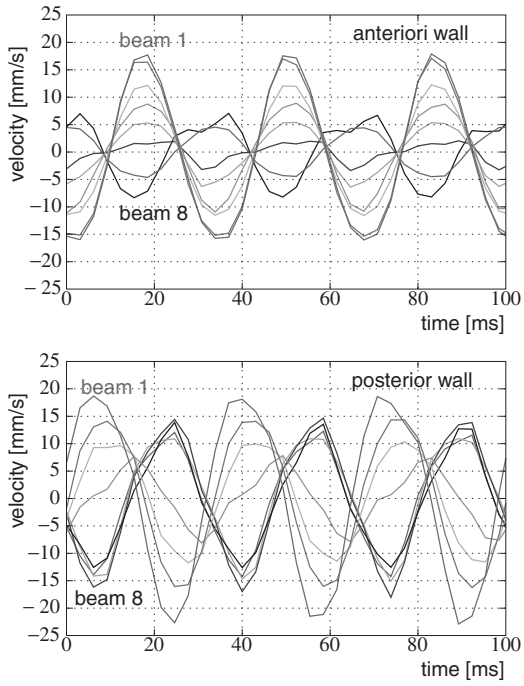

Fig. 4. Waveforms of velocity signals simultaneously measured at eight points on anterior wall and eight points on posterior wall by setting probe at position C.

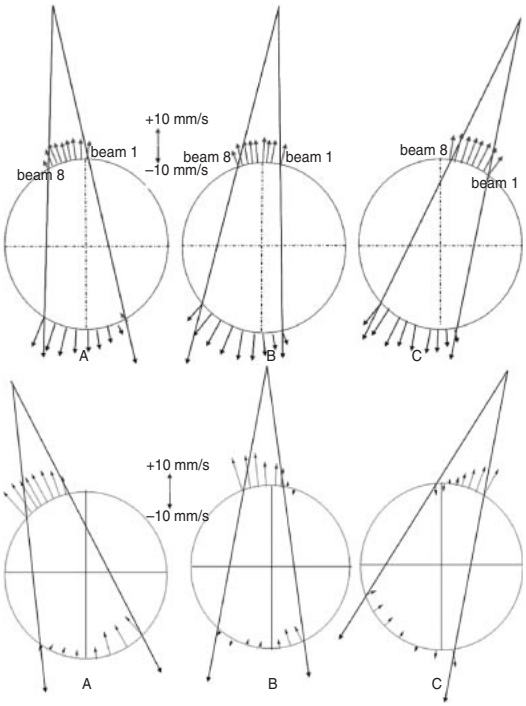

Fig. 5. Amplitude of each vibration waveform at 48 points, detected at time of 18 ms in Fig. 4. Upper: $f_0 = 17$ Hz. Lower: $f_0 = 30$ Hz.

4. *In Vivo* Experiments

By applying the external remote actuator shown in Fig. 2 to the brachial artery of a healthy male subject (32 year old), LV internal pressure was successfully perturbed with mode-0 vibration. The f_0 was approximately 9 Hz, which corresponds to mode 0 in Fig. 4. There was sufficient reproducibility. The motion of the heart wall as measured from the chest wall using the ultrasound-based *phased tracking method*.[10,11] Figure 7 shows a cross-sectional image of the heart and the employed beam direction.

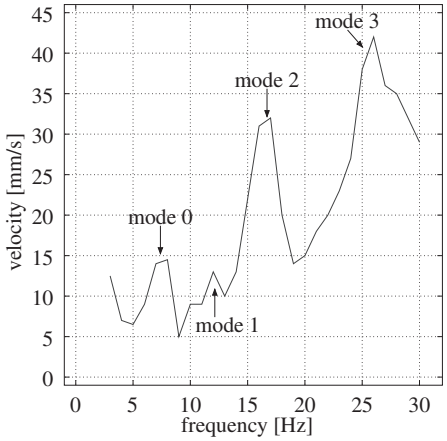

Fig. 6. Maximum amplitude of velocity waveform measured for each applied f_0.

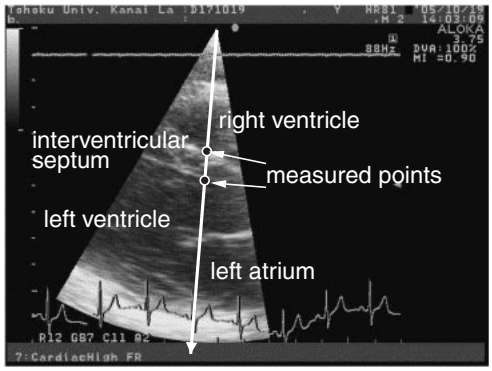

Fig. 7. Cross-sectional image of heart and employed beam direction.

Figures 8(e) and 8(f) show typical waveforms of the velocity signals during the actuation $\{v_{act}(t;i)\}$ $(i = \mathrm{LV}, \mathrm{RV})$ and the cessation of the actuation $\{v_{ces}(t;i)\}$ $(i = \mathrm{LV}, \mathrm{RV})$ on both sides, that is, the right-ventricle (RV) side and the LV side of the IVS during one cardiac cycle. Figure 8(g) shows typical waveforms of the change in the thickness of the IVS during the actuation $\{h_{act}(t)\}$ and the cessation of the actuation $\{h_{ces}(t)\}$, which are obtained by integrating the differences between these velocity signals on both sides of the IVS. The red lines and blue lines in Figs. 8(c)–8(g) show the vibrations or change in thickness measured when the brachium artery was actuated and when it was not actuated, respectively.

Each of the velocity signals was averaged during the actuation $\{v_{act}(t;i)\}$ $(i = \mathrm{LV}, \mathrm{RV})$ and the cessation of the actuation $\{v_{ces}(t;i)\}$ $(i = \mathrm{LV}, \mathrm{RV})$, and the averaged differences, $\{\overline{\Delta v}(t;i) = \overline{v_{act}}(t;i) - \overline{v_{ces}}(t;i)\}$ $(i = \mathrm{LV}, \mathrm{RV})$, between these averaged velocity signals, $\{\overline{v_{act}}(t;i)\}$ $(i = \mathrm{LV}, \mathrm{RV})$ and $\{\overline{v_{ces}}(t;i)\}$ $(i = \mathrm{LV}, \mathrm{RV})$, are shown by solid lines for the RV and LV sides in Figs. 9(c) and 9(d), respectively. The broken lines in Figs. 9(c) and 9(d) show the actuation signal that drives the actuator. By comparing these signals, the difference (solid lines) almost corresponds to the actuation signal (broken lines) particularly during systole (marked at three times by arrows) as shown in Figs. 9(c) and 9(d).

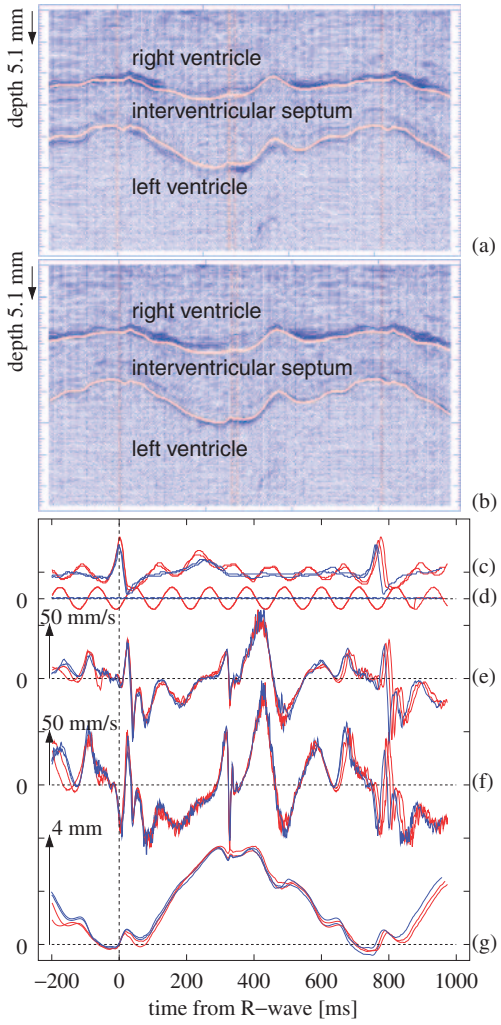

Fig. 8. Waveforms during four cardiac cycles in *in vivo* experiments. (a) M-mode and tracking lines (red) with actuation. The f_0 is 9 Hz. (b) M-mode and tracking lines (red) without actuation. (c) ECG. (d) Actuation signals. (e) Velocity signals $\{v_{act}(t;\mathrm{RV})\}$ and $\{v_{ces}(t;\mathrm{RV})\}$ at RV side of IVS. (f) Velocity signals $\{v_{act}(t;\mathrm{LV})\}$ and $\{v_{ces}(t;\mathrm{LV})\}$ at LV side of IVS. (g) Change in thickness $\{h_{act}(t)\}$ and $\{h_{ces}(t)\}$ of IVS. For (c)–(g), the red lines correspond to the experiments with actuation and blue lines correspond to the experiments with cessation of the actuation.

In a similar way, for the change in thickness, the averaged difference $\overline{\Delta h}(t)$ between $\{h_{act}(t)\}$ and $\{h_{ces}(t)\}$ is shown by a solid line in Fig. 9(e). By comparing the solid line with the broken line in Fig. 9(e), the change in thickness $\overline{\Delta h}(t)$ (solid line) has an almost opposite phase to that of the actuation signal (broken line) at the times marked by arrows.

For f_0 of 9 Hz, the minute velocity components of 5 mm/s due to the perturbation in Figs. 9(c) and 9(d) of the internal pressure were superposed on the spontaneous myocardial motion of approximately 50 mm/s in Figs. 8(e) and 8(f). Also, for the change in thickness of the IVS, minute changes in thickness of approximately 200 μm were superposed on spontaneous changes in thickness of approximately 4 mm in Fig. 8(g). The ratio of the change in thickness caused by remote actuation to the spontaneous change in thickness is approximately 1 : 20 and the pulse pressure is approximately 40 mmHg. Thus, the change in pressure in the LV caused by remote actuation is approximately 2 mmHg. A similar change in pressure has been measured for the CCA using the same remote actuation system in *in vivo* experiments.[8)]

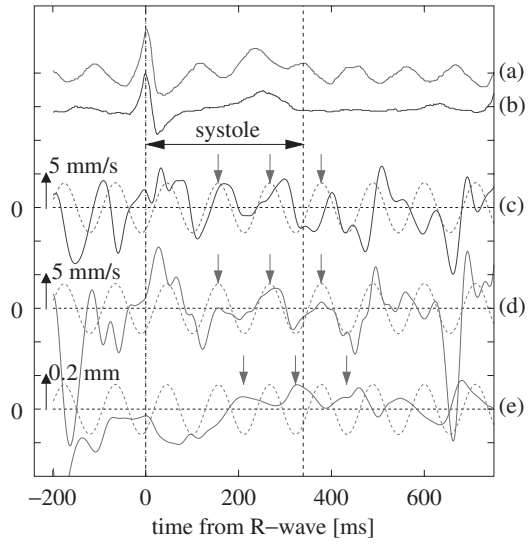

Fig. 9. Difference between waveforms respectively averaged during actuation and cessation in Fig. 8. The broken lines: the averaged actuation signals which electrically drives the actuator. (a) ECG with actuation. (b) ECG without actuation. (c) Averaged difference (solid line) $\overline{\Delta v}(t;\mathrm{RV})$ between velocity signals $\overline{v_{act}}(t;\mathrm{RV})$ and $\overline{v_{ces}}(t;\mathrm{RV})$ at RV side of IVS respectively averaged during actuation and cessation. (d) Averaged difference (solid line) $\overline{\Delta v}(t;\mathrm{LV})$ between velocity signals $\overline{v_{act}}(t;\mathrm{LV})$ and $\overline{v_{ces}}(t;\mathrm{LV})$ at LV side of IVS respectively averaged during actuation and cessation. (e) Averaged difference (solid line) $\overline{\Delta h}(t)$ between averaged changes in thickness, $\overline{h_{act}}(t)$ and $\overline{h_{ces}}(t)$, of IVS averaged during actuation and cessation.

During systole, the aortic valve is open so the perturbation of the internal pressure due to actuation at the brachial artery passes through the aortic valve and propagates into the LV.

5. Conclusions

In this study, we propose a novel method of non-invasively perturbing the LV internal pressure by remotely actuating the brachium artery with sinusoidal vibration. By measuring the spatial distribution of phantom motion using an ultrasound-base method, the vibration mode is identified, which has the potential for non-invasively evaluating the myocardial movability and the transition properties of the heart during the cardiac cycle.

1) L. Loeffler, III and K. Sagawa: Circ. Res. **36** (1975) 498.
2) J. G. Pinto and P. J. Patitucci: Trans. ASME, J. Biomech. Eng. **102** (1980) 57.
3) T. J. Fraites Jr., A. Saeki and D. A. Kass: Circulation **96** (1997) 4408.
4) M. Fatemi, L. E. Wold, A. Alizad and J. F. Greenleaf: IEEE Trans. Med. Imaging **21** (2002) 1.
5) K. Nightingale, M. S. Soo, R. Nightingale and G. Trahey: Ultrasound Med. Biol. **28** (2002) 227.
6) K. Michishita, H. Hasegawa and H. Kanai: Jpn. J. Appl. Phys. **42** (2003) 4608.
7) H. Hasegawa, H. Kanai, Y. Koiwa and J. P. Butler: Jpn. J. Appl. Phys. **42** (2003) 3255.
8) H. Hasegawa and H. Kanai: Jpn. J. Appl. Phys. **43** (2004) 3197.
9) H. Hasegawa and H. Kanai: Jpn. J. Appl. Phys. **44** (2005) 4609.
10) H. Kanai, M. Sato, Y. Koiwa and N. Chubachi: IEEE Trans. Ultrason. Ferroelectr. Freq. Control **43** (1996) 791.
11) H. Kanai, H. Hasegawa, N. Chubachi, Y. Koiwa and M. Tanaka: IEEE Trans. Ultrason. Ferroelectr. Freq. Control **44** (1997) 752.
12) H. Kanai and Y. Koiwa: Ultrasound Med. Biol. **27** (2001) 481.
13) H. Kanai: IEEE Trans. Ultrason. Ferroelectr. Freq. Control **51** (2005) 1931.